

Article

Formation of Yolk–Shell MoS₂@void@Aluminosilica Microspheres with Enhanced Electrocatalytic Activity for Hydrogen Evolution Reaction

Li Li ^{1,2,†} , Yuanyuan Zhao ^{1,†}, Nanli Qiao ³, Zhengbao Yu ³ and Yongxing Zhang ^{1,4,*} 

¹ Anhui Province Key Laboratory of Pollutant Sensitive Materials and Environmental Remediation, Department of Materials Science and Engineering, Huaibei Normal University, Huaibei 235000, China

² Laboratory of Dielectric Functional Materials, School of Materials Science & Engineering, Anhui University, Hefei 230601, China

³ Greenstar (Beijing) Environmental Technology Co., Ltd., Beijing 100176, China

⁴ Department of Chemistry, University of Science and Technology of China, Hefei 230026, China

* Correspondence: zyx07157@mail.ustc.edu.cn

† These authors contributed equally to this work.

Abstract: The development of low-cost electrode materials with enhanced activity and favorable durability for hydrogen evolution reactions (HERs) is a great challenge. MoS₂ is an effective electrocatalyst with a unique layered structure. In addition, aluminosilica shells can not only provide more hydroxyl groups but also improve the durability of the catalyst as a protective shell. Herein, we have designed a hard-template route to synthesize porous yolk–shell MoS₂@void@Aluminosilica microspheres in a NaAlO₂ solution. The alkaline solution can directly etch silica (SiO₂) hard templates on the surface of MoS₂ microspheres and form a porous aluminosilica outer shell. The electrocatalytic results confirm that the MoS₂@void@Aluminosilica microspheres exhibit higher electrocatalytic activity for HERs with lower overpotential (104 mV at the current density of -10 mA cm^{-2}) and greater stability than MoS₂ microspheres. The superior electrocatalytic activity of MoS₂@void@Aluminosilica microspheres is attributed to the unique structure of the yolk@void@shell geometric construction, the protection of the aluminosilica shell, and the greater number of active sites offered by their nanosheet subunits. The design of a unique structure and new protection strategy may set up a new method for preparing other excellent HER electrocatalytic materials.

Keywords: yolk–shell; MoS₂@void@Aluminosilica microspheres; hydrogen evolution reaction; hydrothermal and hard template method



Citation: Li, L.; Zhao, Y.; Qiao, N.; Yu, Z.; Zhang, Y. Formation of Yolk–Shell MoS₂@void@Aluminosilica Microspheres with Enhanced Electrocatalytic Activity for Hydrogen Evolution Reaction. *Energies* **2022**, *15*, 9031. <https://doi.org/10.3390/en15239031>

Academic Editors: Shun Lu, Xiaohui Yang and Yucheng Wang

Received: 7 November 2022

Accepted: 25 November 2022

Published: 29 November 2022

Publisher's Note: MDPI stays neutral with regard to jurisdictional claims in published maps and institutional affiliations.



Copyright: © 2022 by the authors. Licensee MDPI, Basel, Switzerland. This article is an open access article distributed under the terms and conditions of the Creative Commons Attribution (CC BY) license (<https://creativecommons.org/licenses/by/4.0/>).

1. Introduction

Over the past few decades, hydrogen, in particular, sustainable hydrogen production from water splitting, as a clean and renewable energy has received great attention regarding its potential to solve many environmental problems caused by fossil energy [1–5]. For an electrochemical hydrogen evolution reaction (HER), an excellent catalyst should possess lower overpotential and good stability in this important electrochemical process [6,7]. However, highly efficient HER electrocatalysts are Pt-based metals with higher cost and scarcity on the earth, which limits their widespread application [8–11]. Therefore, it is urgent to design an inexpensive and earth-abundant electrocatalyst to replace Pt-based metals and achieve lower overpotential and remarkable reaction kinetics.

In recent years, as an important family of functional materials, nanostructured transition metal sulfides have received intensive research interest due to their electrical conductivity and rich redox electrochemistry [12,13]. Among them, MoS₂, which is one of the layered transition metals dichalcogenides, has received more and more attention in diverse applications, such as solar cells [14], homogeneous biomolecules detection [15],

photodetectors [16], sodium-ion batteries [17], and hydrogen storage [18]. In addition, the structure of the material is also an important factor affecting its performance. Taking these two factors (the material of MoS₂ and the structure) into account, preparing MoS₂ micro- and nanostructures with controllable morphologies and sizes has attracted lots of attention. For example, three-dimensional (3D) MoS₂ nanoflowers with large stretched “thin folding leaves” and considerable nanopores were synthesized by a polypyrrole-assisted one-pot hydrothermal routine [19]; nanostructured MoS₂ particles on a 3D carbon fiber paper substrate with preferentially exposed edge sites were successfully synthesized by the facile pyrolysis and sulfurization methods [20]; 2D MoS₂ monolayers with defect structures were prepared by direct sulfurization and chemical vapor deposition (CVD) [21]; a type of prickly-pear-like 3D porous MoS₂ was hydrothermally synthesized (ZT-MoS₂) with a zinc oxide (ZnO) rod template which deposited on quartz glass substrates [22]; zinc-doped MoS₂ material was prepared by a facile solvothermal method and using (NH₄)₂MoS₄ as precursors in DMF solution [23]; and an edge-rich MoS₂ nanoarray grown on an edge-oriented 3D graphene was prepared via CVD [24]. Although various reasonable progressions have been carried out in designs of the structure, there are still some inadequacies, such as complicated operation with inefficient catalytic activity and instability. In addition to the structures above, as a special extension of core-shell systems, the yolk-shell structure exhibits a distinctive yolk@void@shell configuration with an interspace between the core and porous shell (in most cases) which can provide a protective route for buffering the volume change and thus enhance the stability of the material [25]. For example, Wang et al. reported that yolk-shell ZnS@NC@MoS₂ nanoboxes can provide increased active sites and ion channels among the interfacial boundaries, high conductivity, and a stable structure for the sodium ion batteries (SIBs) anode [26]. However, MoS₂ electrocatalysts with aluminosilica protective shells have not been reported. Therefore, it is highly desirable to develop a facile and cost-efficient method to fabricate MoS₂-based catalysts with efficient catalytic performance and great stability.

In this work, we report that MoS₂@void@Aluminosilica microspheres with porous shells are prepared by a facile and robust method. In this experiment, SiO₂, which is first modified the surface of MoS₂ microspheres assembled by nanosheets, induced preferential generation and deposition of the porous aluminosilica shell. According to our research, this is the first report on the fabrication and electrocatalytic activity for HERs of monodispersed MoS₂@void@Aluminosilica microspheres. Most importantly, as an efficient electrocatalyst, MoS₂@void@Aluminosilica microspheres possess the following three features: (1) larger specific areas offered by their nanosheet subunits can provide more active sites for HER processes; (2) electrochemical kinetics are enhanced by the short diffusion lengths between the hierarchical MoS₂ microsphere core and the aluminosilica shell; (3) HER stability benefited from the porous aluminosilica shell.

2. Materials and Methods

2.1. Preparation of Hierarchical MoS₂ Microspheres Assembled by Nanosheets

In this experiment, 0.1 g of thioacetamide (TAA, 99%) and sodium molybdate (Na₂MoO₄·2H₂O, 99%, 0.3 g) were dispersed in deionized (DI) water with continuous magnetic stirring. After 15 min, 0.2 g of polyethylene-polypropylene glycol, F68 (referred to as F68) was added to the mixed solution and stirred for 20 min. Then, the above solution was transferred to the 50 mL Teflon-lined, stainless-steel autoclave and kept at 180 °C for 12 h. When the autoclave was cooling down, the powder was washed with DI water and absolute ethanol three times and finally dried in a vacuum oven at 60 °C for 12 h.

2.2. Preparation of MoS₂@SiO₂ Microspheres

The SiO₂ was prepared on the basis of the Stöber method with some modification [27]. Briefly, 0.05 g of as-prepared MoS₂ microspheres was dispersed into a mixture solution including 20 mL ethanol and 4 mL deionized water under ultrasonication for 20 min. Then, 0.2 mL of tetraethyl orthosilicate (TEOS) and 0.25 mL of ammonia solution (25%) were

added to above solution and stirred for 3.5 h. The obtained products were washed with DI water and ethanol then dried under vacuum at 60 °C for 10 h.

2.3. Preparation of MoS₂@void@Aluminosilica Microspheres

The synthesis process of MoS₂@void@Aluminosilica microspheres was carried out according to our previous work [28], which is described briefly as follows: The MoS₂@SiO₂ microspheres (50 mg) were dispersed in 10 mL of DI water to form homogeneous solution A. A total of 0.05 g of sodium aluminate (NaAlO₂) was dissolved into 20 mL of DI water to form solution B. Then, solution A was poured into solution B to form a homogeneous suspension and then transferred to a Teflon autoclave (50 mL) and heated at 140 °C for 4 h. After cooling down to room temperature, the product was washed and dried in a vacuum oven at 60 °C overnight.

2.4. Electrochemical Measurements

The electrochemical property of the as-prepared samples was obtained by using a three-electrode system connected to a CHI 760E electrochemical workstation (Shanghai Chenhua Instrument Co., Shanghai, China). A total of 5 mg of as-prepared samples together with 10 µL of Nafion solution was dispersed into 800 µL of ethanol and 200 µL of distilled water and sonicated for 30 min to form a homogeneous ink. Then, the ink was pipetted onto the FTO-coated glass and then used as the working electrodes. The Ag/AgCl electrode was employed as the reference electrode and a platinum plate as the counter electrode, and the 0.5 M H₂SO₄ solution was employed as electrolyte in all electrochemical tests. All of the electrochemical measurements were performed in a three-electrode system at room temperature. Linear sweep voltammetry (LSV) was conducted from 0 to −0.4 V versus (vs.) reversible hydrogen electrode (RHE) with a scan rate of 5 mV s^{−1} at room temperature. Electrochemical impedance spectroscopy (EIS) measurement was conducted at the overpotential of 500 mV with a potential perturbation of 5 mV amplitude in the range from 10⁶ Hz to 0.1 Hz. All potentials measured vs. Ag/AgCl were converted to RHE using the following equation:

$$E_{\text{RHE}} = E_{\text{Ag/AgCl}} + 0.059 \text{ pH} + E_{\text{Ag/AgCl}}^{\theta} \quad (1)$$

where E_{RHE} is the converted potential vs. RHE, $E_{\text{Ag/AgCl}}$ is the measured potential vs. the Ag/AgCl electrode, and $E_{\text{Ag/AgCl}}^{\theta} = 0.1976 \text{ V}$ at 25 °C.

2.5. Characterization

X-ray diffraction (XRD) patterns were measured on a Philips X'Pert Pro X-ray diffractometer (Holland Panalytical, Almelo, The Netherlands) with Cu K α radiation (1.5418 Å). The main samples were characterized by taking TEM images using a JEOL JEM-2100 microscope (Hitachi Co., Tokyo, Japan). Scanning electron microscope (SEM) images were carried out at a SEM (Quanta 200 FEG, Tokyo, Japan) with an accelerating voltage of 10.0 kV. Specific surface areas of the samples were tested by Brunauer–Emmet–Teller (BET, Micromeritics ASAP 2020 M+C, Micromeritics Instrument Co., Atlanta, GA, USA) equipped with nitrogen adsorption and desorption. The static water contact angle (CA) measurement was tested on an optical CA meter system (Data Physics Instrument GmbH, Filderstadt, Germany).

3. Results and Discussion

The fabrication process for the MoS₂@void@Aluminosilica is shown in Figure 1. Firstly, the reactions of Na₂MoO₄ and S^{2−} released from the TAA by hydrothermal method treatment at 180 °C formed the MoS₂ nanosheets. In addition, the MoS₂ nanosheets spontaneously assembled into MoS₂ microspheres with the addition of F68. In our experiments, it is supposed that the F68 intertwines to form a network structure in the solution and adsorbs on the surface of MoS₂ nanosheets due to the strong interaction between MoS₂ and

F68. Thus, the MoS₂ nanosheets encapsulated by F68 assembled to the MoS₂ microspheres in order to decrease the surface energy [29]. Secondly, SiO₂ was coated as the shell on the surface of the MoS₂ microspheres (MoS₂@SiO₂ microspheres) via the Stöber method at room temperature (TEOS as the SiO₂ source in alkaline solution was used in the reaction process). Finally, NaAlO₂ aqueous solution was employed as an alkaline solution to etch SiO₂ hard templates on the surface of the MoS₂ microspheres to form the monodispersed MoS₂@void@Aluminosilica microspheres with porous aluminosilica shell structures via the hydrothermal method at 140 °C.



Figure 1. Schematic illustration for the synthesis of the MoS₂@void@Aluminosilica microspheres.

The phase structures of the as-prepared products are tested with XRD (Figure 2). The XRD pattern of the MoS₂ sample shows that all the main diffraction peaks can be indexed to the (002), (100), (102), and (110) plane of the hexagonal MoS₂ phase (JCPDS No. 37–1492, P63/mmc). The (002) plane located at ~13.9° especially indicates that the MoS₂ is the graphene-like structure, and its corresponding *d* spacing is 0.62 nm, which was calculated based on Bragg's equation. However, other peaks that slightly shift toward a lower angle of the diffraction peaks can be found. The reason for this phenomenon is caused by lattice strains derived from the folding and bending of the layers [30]. The typical XRD patterns of the MoS₂@SiO₂ microspheres and the MoS₂@void@Aluminosilica microspheres show almost the same features as those shown in MoS₂. There are no other diffraction peaks that can correspond to SiO₂ and aluminosilica because SiO₂ and aluminosilica are amorphous [28].

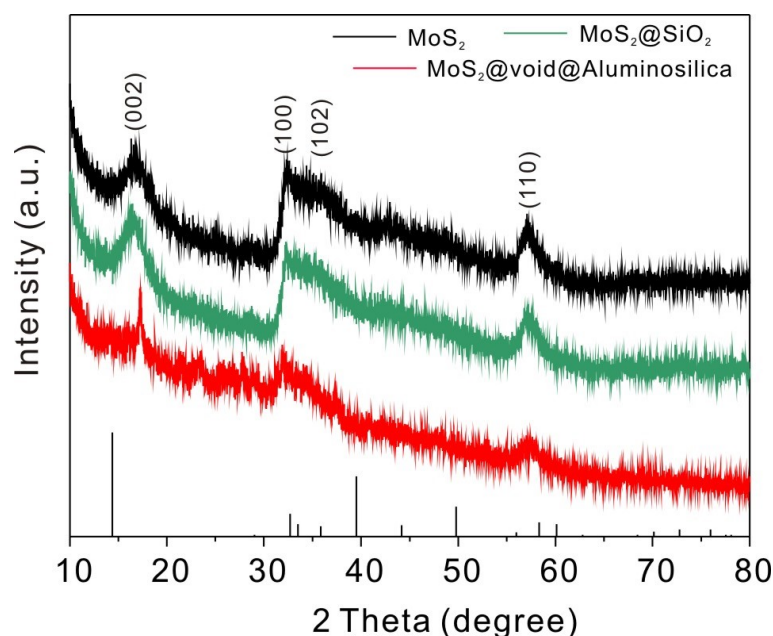


Figure 2. XRD pattern of the MoS₂ microspheres, the MoS₂@SiO₂ microspheres, and the MoS₂@void@Aluminosilica microspheres.

As shown in Figure 3a, as we can see, the MoS₂ was assembled by many monodispersed spherical particles with an average diameter of ~300 nm, which could work as seeds for further coating the SiO₂ shell on the surface of the MoS₂ microspheres to form core-shell composites [31]. The MoS₂ microspheres were further investigated by the TEM in Figure 3b,c, from which we found that the MoS₂ microspheres were assembled by nanosheets with a thickness of ~5.0 nm. As shown in Figure 3d, the MoS₂@SiO₂ microspheres possess a smooth SiO₂ shell, and the average particle diameter of the sample increased from 300 to 400 nm, which suggests that the thick shell of SiO₂ with ~100 nm was successfully coated onto the surface of the MoS₂ microspheres. TEM images in Figure 3e,f also suggest that the SiO₂ shell was successfully coated on the surface of the MoS₂ microspheres. In addition, the thickness of the shell was about 85 nm (Figure 3f). The aluminosilica shell and the MoS₂ core can be seen clearly in Figure 3g,h; the MoS₂@void@Aluminosilica microspheres possess yolk-void-shell structures. It is worth noticing that the SiO₂ shell is the key process for synthesizing MoS₂@void@Aluminosilica microspheres because the SiO₂ shell can induce the preferential generation and deposition of porous aluminosilica shells [28]. Compared to the MoS₂@SiO₂ microspheres with core-shell structure (Figure 3e,f), there is a clearer boundary between the outer aluminosilica shell, MoS₂ core, and the void space of MoS₂@void@Aluminosilica microspheres in the yolk-shell structures in Figure 3i. In addition, the SEM and TEM images of the SiO₂ microspheres are shown in Figure S1, and the SEM and TEM images of the hollow aluminosilica microspheres are shown in Figure S2. These aspects can be viewed in the Supplementary Materials.

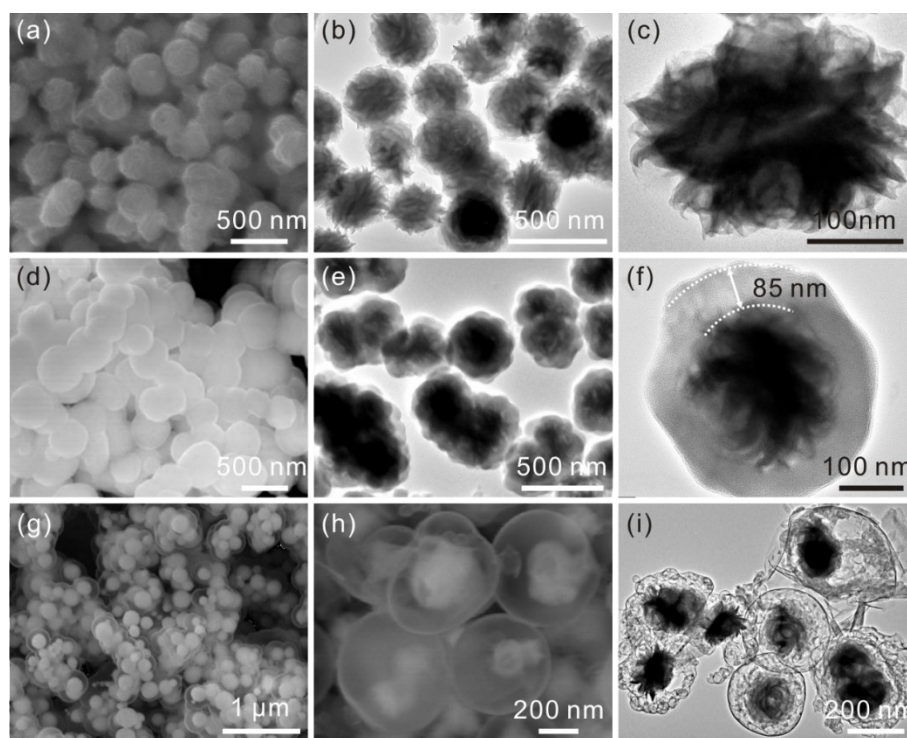


Figure 3. SEM and TEM images of (a–c) the MoS₂ microspheres, (d–f) the MoS₂@SiO₂ microspheres, (g–i) the MoS₂@void@Aluminosilica microspheres.

The high-magnification TEM images of the MoS₂@void@Aluminosilica microspheres are shown in Figure 4a,b. In addition, Figure 4b shows that there are many mesopores (black circles) in the shell of the as-prepared sample. As shown in Figure 4i, the thickness of the shell of MoS₂@void@Aluminosilica microspheres is about 20 nm. Additionally, Figure 4i further reveals that the outer aluminosilica shell is amorphous, which is consistent with the SAED pattern (see inset of Figure 4i) and the XRD pattern (Figure 2). The HRTEM image (Figure 4k) shows that the MoS₂ core has a typical layered structure with interlayer

spacing at 0.62 nm, which corresponds to the (002) plane of hexagonal MoS₂ (JCPDS No. 37-1492). In addition, the electron mapping images in Figure 4c–h indicate Si-, O-, Al-, Na-, Mo-, and S-enriched areas of the MoS₂@void@Aluminosilica microspheres, respectively. The EDS analysis (Figure 4j) of the MoS₂@void@Aluminosilica microspheres further reveals the existence of Si, O, Al, Na, Mo, and S elements.

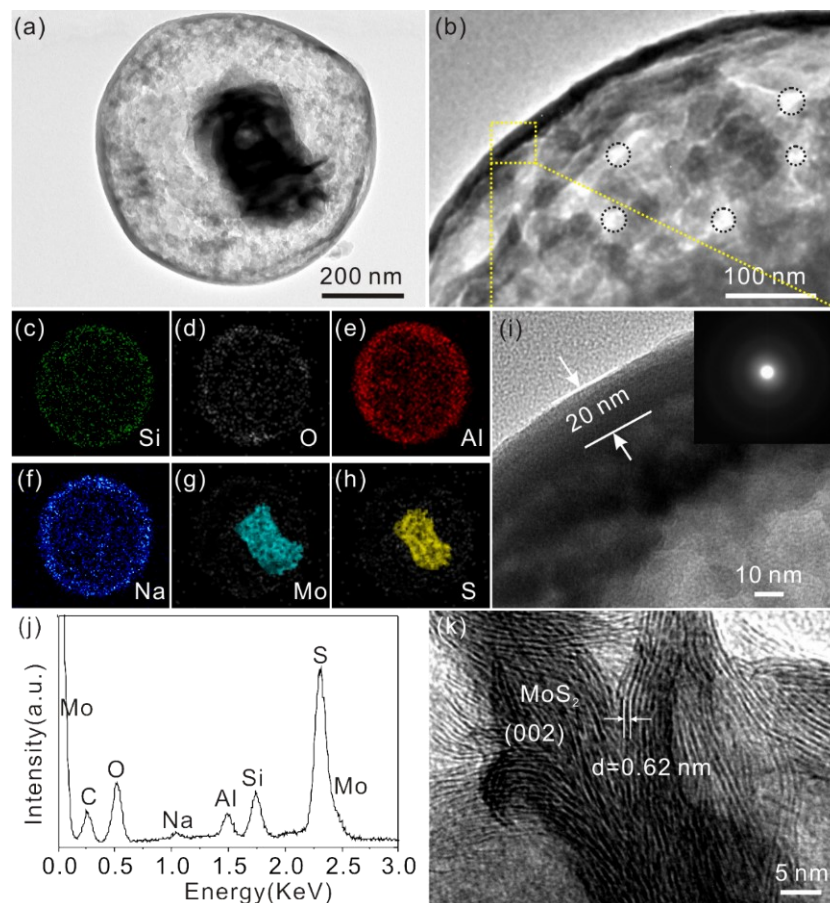


Figure 4. The images of the MoS₂@void@Aluminosilica microspheres: (a,b) low-magnification TEM images; electron energy loss: (c) “Si”, (d) “O”, (e) “Al”, (f) “Na”, (g) “Mo” and (h) “S”; (i) HRTEM image and the corresponding SAED pattern (inset in (i)); (j) EDS spectrum; (k) HRTEM image.

As shown in Figure 5, the MoS₂ microspheres and the MoS₂@void@Aluminosilica microspheres are of type IV isotherms, which indicates that both of them possess meso/microporous structures. The pore-size distribution curve of the MoS₂ microspheres shows a broad peak from 2–105 nm with a maximum of 90 nm. The MoS₂@void@Aluminosilica microspheres exhibit the same broad peak range but with a maximum of 85 nm. These results indicate that there are many mesopores/macropores in the above two mentioned samples. In addition, the mesopores may reflect the space between the nanosheets which assemble the MoS₂ microspheres or the MoS₂@void@Aluminosilica microspheres, while larger macropores can be concerned with the space between the MoS₂ microspheres or the MoS₂@void@Aluminosilica microspheres. For the MoS₂@void@Aluminosilica microspheres especially, larger mesopores may index to the void space between the yolk and shell of the sample, while the smaller mesopores can reflect the porosity of the aluminosilica shell. However, the porosity of the MoS₂@SiO₂ microspheres can be neglected.

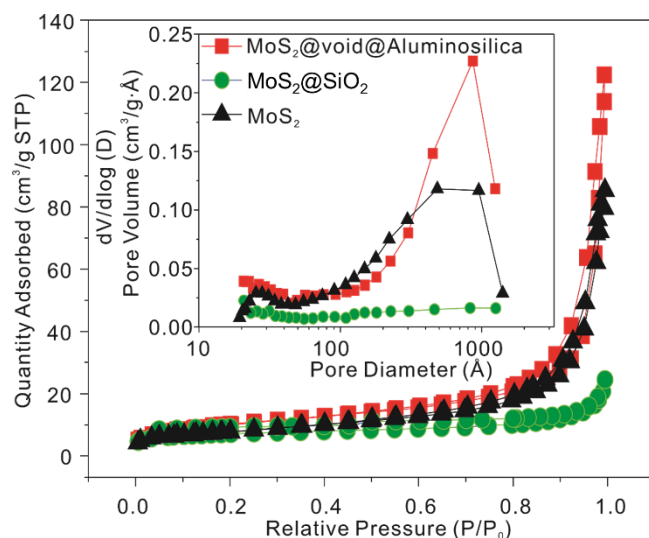


Figure 5. Nitrogen adsorption–desorption isotherms and the corresponding pore-size distribution curves (inset) of the MoS₂ microspheres, the MoS₂@SiO₂ microspheres, and the MoS₂@void@Aluminosilica microspheres.

The BET surface areas, average pore diameters, and pore volumes of the three main as-synthesized samples are summarized in Table 1. From the data, it can be clearly seen that the MoS₂ microspheres possess a large specific surface area and a bigger pore volume. After the SiO₂ was coated on the surface of the MoS₂ microspheres, the MoS₂@SiO₂ microspheres possessed the smallest specific surface area and pore volume, which indicates that solid SiO₂ reduced the amount of exposure active sites and blocked the ion channel. After being etched by an alkaline solution, the MoS₂@void@Aluminosilica microspheres possessed larger BET and higher pore volume, which indicates the porous aluminosilica shell can provide more exposure to active sites and more open ion channel.

Table 1. Some physical properties of the three main samples.

Samples	BET (m ² /g)	Average Pore Diameter (Å)	Pore Volume (cm ³ /g)
MoS ₂	27.35	140.5	0.096
MoS ₂ @SiO ₂	24.96	40.8	0.025
MoS ₂ @void@Aluminosilica	36.49	110.0	0.100

As shown in Figure 6, a typical three-electrode system was employed to evaluate the HER performance of the as-prepared samples in the H₂SO₄ electrolyte. Figure 6a presents the LSV measurements performed at 5 mV s^{−1}. The MoS₂@void@Aluminosilica microspheres' electrode showed a lower overpotential of 104 mV at a current density of −10 mA cm^{−2} while the MoS₂ microspheres were 127 mV. In addition, the SiO₂ microspheres, the hollow aluminosilica microspheres, and the MoS₂@SiO₂ microspheres exhibited negligible electrocatalytic activities for HERs. The results show that the as-synthesized MoS₂@void@Aluminosilica microspheres hold great promise for electrocatalytic hydrogen evolution. The kinetics of the catalytic HER was commonly investigated and quantified by the Tafel slope, which can be readily determined from the LSV curves by recasting the data into the Tafel equation:

$$\eta = b \times \log |j| + a \quad (2)$$

with *b* being the Tafel slope and *j* being the current density (mA cm^{−2}). A smaller Tafel slope means a faster-increased rate of the HER with a rising potential [32]. As shown in Figure 6b, the Tafel slope of MoS₂@void@Aluminosilica microspheres was 123 mV dec^{−1}, which is lower than that of the MoS₂ microspheres (169 mV dec^{−1}), the MoS₂@SiO₂ microspheres (197 mV dec^{−1}), the SiO₂ microspheres (214 mV dec^{−1}), and the hollow aluminosilica microspheres (223 mV dec^{−1}), respectively, indicating the outstanding kinetic

performance of the MoS₂@void@Aluminosilica microspheres. The decrease of the Tafel slope for the MoS₂@void@Aluminosilica microspheres may be attributed to the formation of the aluminosilica shell on the surface of the MoS₂ microspheres as evidenced by their corresponding SEM and TEM morphologies because of the reduced corrosion of MoS₂ core. In addition, Table 2 presents a thorough overview of the reporting MoS₂-based materials toward the electrochemical property. Obviously, there are many methods to prepare MoS₂ electrocatalysts; however, the MoS₂@void@Aluminosilica microspheres in this work possess better performance than others. This much-enhanced electrocatalytic performance is also supported by the electrochemical impedance spectroscopy (EIS) in Figure 6c; the equivalent circuit diagram is shown in Figure S3. The impedance of the MoS₂@void@Aluminosilica microspheres was found to be much smaller than that of the MoS₂ microsphere and other samples (the SiO₂ microspheres, the hollow aluminosilica microspheres, and the MoS₂@SiO₂ microspheres, as shown in Figure S4), which is ascribed to the unique structure of the yolk@void@shell geometric construction, the presence of aluminosilica shell helps to adsorb the reactants in the solution, the greater number of active sites offered by their nanosheet subunits, and the enhancement of the hydrophilicity. It can be concluded that the MoS₂@void@Aluminosilica microsphere exhibits superior electrode kinetics and thus can enhance the electrochemical HER activity. As shown in Figure S5, the MoS₂@void@Aluminosilica microspheres show a capacitance value of up to 0.66 mF cm⁻², which is slightly lower than that of MoS₂ electrodes (0.67 mF cm⁻²). The electrochemical active surface area (ECSA) of the MoS₂@void@Aluminosilica microspheres was 16.5 cm² while MoS₂ was 16.7 cm², indicating that the Aluminosilica shell cannot decrease the active surface area of MoS₂. To investigate the HER stability of the MoS₂@void@Aluminosilica microspheres, a long-term potential cycling test was performed at a scan rate of 10 mV s⁻¹. As shown in Figure 6d, only a slight activity loss of the MoS₂@void@Aluminosilica microspheres was observed, even after 500 continuous cycles, while there was a significant decline in potentials for the MoS₂ microspheres, which may be attributed to the MoS₂ core not corroded because it was protected by the aluminosilica shell. In addition, as shown in Figure 6e, after continuous testing at the static current density of -10 mA cm⁻², the potential of the MoS₂@void@Aluminosilica microspheres remained stable for a long period test and showed excellent stability under acidity conditions.

Table 2. The synthesis method and HER performance of the MoS₂-based electrocatalysts.

Catalyst	Synthesis Method	η_{10} (mV) *	Tafel Slope (mV dec ⁻¹)	Ref.
MoS ₂ (activated)	Commercial activated method	—	180	[18]
3D MoS ₂ nanoflowers	Hydrothermal method	350	95.5	[19]
se-MoS ₂	Hydrothermal method	104	59	[33]
r-MoS ₂	Microwave hydrothermal method	217	121	
MoS ₂	Hydrothermal method	340	105	[34]
Zn-MoS ₂	Hydrothermal method	290	110	
MoS ₂ @3DC	Pyrolysis method	252	102.8	[35]
MoS ₂	Hydrothermal method	400	157	[36]
3D MoS ₂	Hard template method	270	112	[37]
MoS ₂	Template sacrificial method	508	136	[38]
MoS ₂ nanosheets	Hydrothermal method	308	201	[39]
MoS ₂ microspheres	Hydrothermal method	127	169	
MoS ₂ @void@Aluminosilica	Hydrothermal and hard template method	104	123	This work

* HER overpotential at -10 mA cm⁻² achieved at a given catalyst loading.

To probe the interface property of the electrocatalyst, the hydrophilicity of the MoS₂@void@Aluminosilica microspheres was investigated. As shown in Figure 6f, the contact angle of the MoS₂@void@Aluminosilica microspheres was 10°, which was smaller than that of the MoS₂ microspheres (27°), suggesting the former has better hydrophilicity than the latter. More hydrophilic surface was conducive to contact between the reactants and active sites, enabling the facile release of evolved H₂ gas bubbles and facilitating electron

transfer to improve water electrolysis [40]. Consequently, all the above results powerfully confirmed that $\text{MoS}_2@\text{void@Aluminosilica}$ microspheres have greatly optimized the HER reaction kinetics and thus significantly enhanced the HER catalytic activity. The improved performance of $\text{MoS}_2@\text{void@Aluminosilica}$ is attributed to the greater number of active sites offered by MoS_2 nanosheet subunits and hydrophilic hydroxyl groups on the surface of aluminosilica.

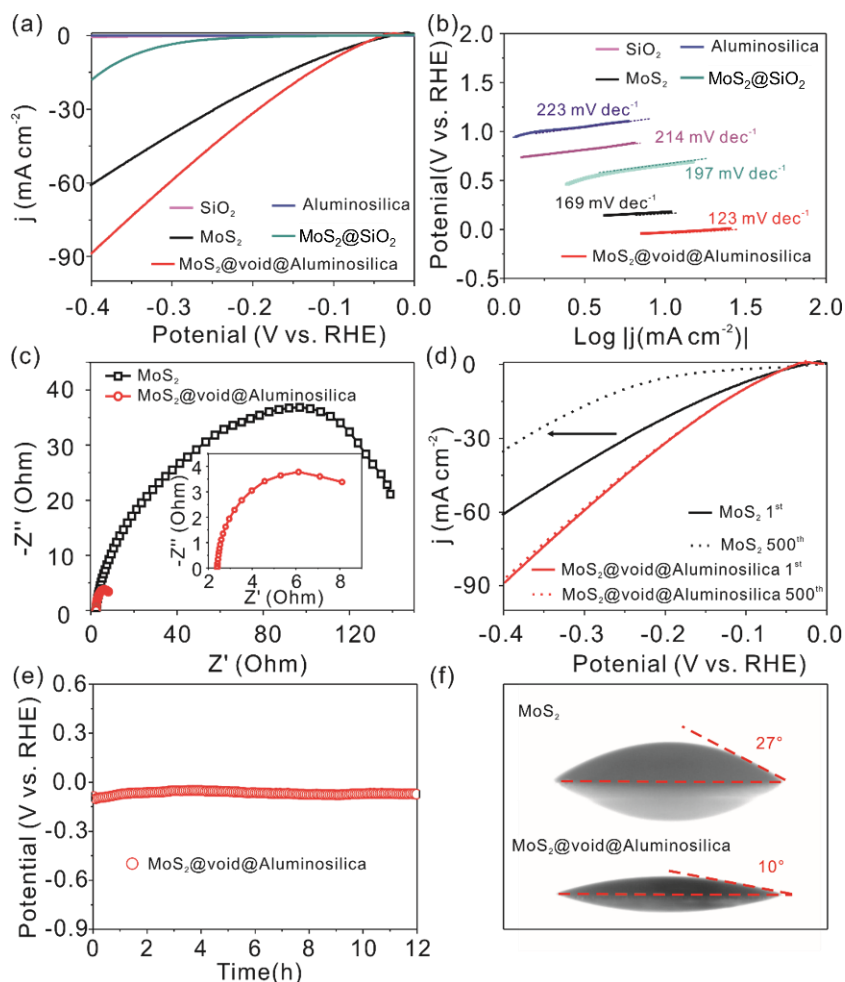


Figure 6. (a) HER polarization curves without iR-compensation; (b) Tafel slopes; (c) EIS; (d) LSV curves for before and after 500 CV cycles; (e) chronopotentiometry curve of the $\text{MoS}_2@\text{void@Aluminosilica}$ microspheres at the constant current density of -10 mA cm^{-2} ; (f) contact angle measurements of the MoS_2 microspheres and the $\text{MoS}_2@\text{void@Aluminosilica}$ microspheres.

4. Conclusions

In conclusion, $\text{MoS}_2@\text{void@Aluminosilica}$ microspheres have been successfully prepared by hydrothermal and hard template methods. The experimental results illustrate that $\text{MoS}_2@\text{void@Aluminosilica}$ microspheres display great electrocatalytic activities and stability for HERs compared with MoS_2 microspheres. The excellent HER catalytic performance of $\text{MoS}_2@\text{void@Aluminosilica}$ microspheres is ascribed to the unique structure of the yolk@void@shell geometric construction, the presence of aluminosilica shell, and the greater number of active sites offered by their nanosheet subunits. The products with the yolk@void@shell structures prepared by the simple protocol and unique protection strategy are prospectively applicable in the fields of electrocatalysis and batteries.

Supplementary Materials: The following supporting information can be downloaded at <https://www.mdpi.com/article/10.3390/en15239031/s1>, Figure S1: SEM (a) and TEM (b) images of SiO₂ microspheres; Figure S2: SEM (a) and TEM (b) images of hollow aluminosilica microspheres; Figure S3: Equivalent circuit diagram (R_s is the solution resistance; C_{dl} is the double layer capacitance; R_{ct} is the charge transfer resistance); Figure S4: Electrochemical impedance spectroscopy of the SiO₂ microspheres, the hollow aluminosilica microspheres, and the MoS₂@SiO₂ microspheres; Figure S5: Plots of the double-layer capacitances of MoS₂ and MoS₂@void@Aluminosilica.

Author Contributions: Conceptualization, Y.Z. (Yongxing Zhang); methodology, L.L. and Y.Z. (Yuanyuan Zhao); software, L.L. and Y.Z. (Yuanyuan Zhao); validation, L.L. and Y.Z. (Yuanyuan Zhao); formal analysis, L.L. and Y.Z. (Yuanyuan Zhao); investigation, L.L. and Y.Z. (Yuanyuan Zhao); resources, L.L. and Y.Z. (Yuanyuan Zhao); data curation, L.L. and Y.Z. (Yuanyuan Zhao); writing—original draft preparation, L.L. and Y.Z. (Yuanyuan Zhao); writing—review and editing, L.L., Y.Z. (Yuanyuan Zhao), N.Q. and Y.Z. (Yongxing Zhang); visualization, Z.Y. and Y.Z. (Yongxing Zhang); supervision, Y.Z. (Yuanyuan Zhao); project administration, Y.Z. (Yongxing Zhang), N.Q. and Z.Y.; funding acquisition, Y.Z. (Yongxing Zhang) and N.Q. All authors have read and agreed to the published version of the manuscript.

Funding: This research was supported by the Key Natural Science Research Project for Colleges and Universities of Anhui Province (Grant No. KJ2021ZD0056), the University Enterprise Joint Research and Development Project (Grant No. GLSD—YFAH.2022001.002), and the Open Project of Anhui Province Key Laboratory of Pollutant Sensitive Materials and Environmental Remediation (Grant No. Not Applicable).

Conflicts of Interest: The authors declare no conflict of interest.

References

1. Wu, Y.; Liu, X.; Han, D.; Song, X.; Shi, L.; Song, Y.; Niu, S.; Xie, Y.; Cai, J.; Wu, S.; et al. Electron density modulation of NiCo₂S₄ nanowires by nitrogen incorporation for highly efficient hydrogen evolution catalysis. *Nat. Commun.* **2018**, *9*, 1425. [[CrossRef](#)] [[PubMed](#)]
2. Zhang, J.-Y.; Wang, H.; Tian, Y.; Yan, Y.; Xue, Q.; He, T.; Liu, H.; Wang, C.; Chen, Y.; Xia, B.Y. Anodic Hydrazine Oxidation Assists Energy-Efficient Hydrogen Evolution over a Bifunctional Cobalt Perselenide Nanosheet Electrode. *Angew. Chem. Int. Ed.* **2018**, *57*, 7649–7653. [[CrossRef](#)] [[PubMed](#)]
3. Lu, S.; Hummel, M.; Gu, Z.; Wang, Y.; Wang, K.; Pathak, R.; Zhou, Y.; Jia, H.; Qi, X.; Zhao, X.; et al. Highly Efficient Urea Oxidation via Nesting Nano-Nickel Oxide in Eggshell Membrane-Derived Carbon. *ACS Sustain. Chem. Eng.* **2021**, *9*, 1703–1713. [[CrossRef](#)]
4. Jia, H.; Lu, S.; Ra Shin, S.H.; Sushko, M.L.; Tao, X.; Hummel, M.; Thallapally, P.K.; Liu, J.; Gu, Z. In Situ anodic electrodeposition of two-dimensional conductive metal-organic framework@nickel foam for high-performance flexible supercapacitor. *J. Power Sources* **2022**, *526*, 231163. [[CrossRef](#)]
5. Fang, L.; Wang, S.; Song, C.; Lu, S.; Yang, X.; Qi, X.; Liu, H. Boosting nitrate electroreduction to ammonia via in situ generated stacking faults in oxide-derived copper. *Chem. Eng. J.* **2022**, *446*, 137341. [[CrossRef](#)]
6. Esposito, D.V.; Hunt, S.T.; Stottlemeyer, A.L.; Dobson, K.D.; McCandless, B.E.; Birkmire, R.W.; Chen, J.G. Low-Cost Hydrogen-Evolution Catalysts Based on Monolayer Platinum on Tungsten Monocarbide Substrates. *Angew. Chem. Int. Ed.* **2010**, *49*, 9859–9862. [[CrossRef](#)] [[PubMed](#)]
7. Xue, F.; Kang, S.; Dai, Y.; Li, T.; Shen, P.K.; Zhu, J.; Lu, S.; Fu, X.; Wang, L.; Feng, S.; et al. Hierarchical lead grid for highly stable oxygen evolution in acidic water at high temperature. *J. Power Sources* **2021**, *493*, 229635. [[CrossRef](#)]
8. Liang, K.; Guo, L.; Marcus, K.; Zhang, S.; Yang, Z.; Perea, D.E.; Zhou, L.; Du, Y.; Yang, Y. Overall Water Splitting with Room-Temperature Synthesized NiFe Oxyfluoride Nanoporous Films. *ACS Catal.* **2017**, *7*, 8406–8412. [[CrossRef](#)]
9. Lu, S.; Wang, Y.; Xiang, H.; Lei, H.; Xu, B.B.; Xing, L.; Yu, E.H.; Liu, T.X. Mass transfer effect to electrochemical reduction of CO₂: Electrode, electrocatalyst and electrolyte. *J. Energy Stor.* **2022**, *52*, 104764. [[CrossRef](#)]
10. Verma, J.; Goel, S. Cost-effective electrocatalysts for Hydrogen Evolution Reactions (HER): Challenges and Prospects. *Int. J. Hydrog. Energy* **2022**, *47*, 38964–38982. [[CrossRef](#)]
11. Zhou, F.; Zhou, Y.; Liu, G.-G.; Wang, C.-T.; Wang, J. Recent advances in nanostructured electrocatalysts for hydrogen evolution reaction. *Rare Met.* **2021**, *40*, 3375–3405. [[CrossRef](#)]
12. Wang, M.; Ju, P.; Li, W.; Zhao, Y.; Han, X. Ag₂S nanoparticle-decorated MoS₂ for enhanced electrocatalytic and photoelectrocatalytic activity in water splitting. *Dalton Trans.* **2017**, *46*, 483–490. [[CrossRef](#)] [[PubMed](#)]
13. Yan, C.; Yang, X.; Lu, S.; Han, E.; Chen, G.; Zhang, Z.; Zhang, H.; He, Y. Hydrothermal synthesis of vanadium doped nickel sulfide nanoflower for high-performance supercapacitor. *J. Alloys Compd.* **2022**, *928*, 167189. [[CrossRef](#)]
14. Zhang, Y.; Yu, W.; Zhai, X.; Liu, Z.; Su, L.; Teng, X.; Fu, G. The effect of oxygen pretreatment at hetero-interface on the photovoltaic properties of MoS₂/Si heterojunction solar cells. *J. Alloys Compd.* **2019**, *803*, 1023–1031. [[CrossRef](#)]

15. Zhu, C.; Zeng, Z.; Li, H.; Li, F.; Fan, C.; Zhang, H. Single-Layer MoS₂-Based Nanoprobes for Homogeneous Detection of Biomolecules. *J. Am. Chem. Soc.* **2013**, *135*, 5998–6001. [[CrossRef](#)]
16. Qiao, S.; Liu, J.; Fu, G.; Wang, S.; Ren, K.; Pan, C. Laser-induced photoresistance effect in Si-based vertical standing MoS₂ nanoplate heterojunctions for self-powered high performance broadband photodetection. *J. Mater. Chem. C* **2019**, *7*, 10642–10651. [[CrossRef](#)]
17. Hu, Z.; Liu, Q.; Chou, S.-L.; Dou, S.-X. Advances and Challenges in Metal Sulfides/Selenides for Next-Generation Rechargeable Sodium-Ion Batteries. *Adv. Mater.* **2017**, *29*, 1700606. [[CrossRef](#)]
18. Kim, Y.; Jackson, D.H.K.; Lee, D.; Choi, M.; Kim, T.-W.; Jeong, S.-Y.; Chae, H.-J.; Kim, H.W.; Park, N.; Chang, H.; et al. In Situ Electrochemical Activation of Atomic Layer Deposition Coated MoS₂ Basal Planes for Efficient Hydrogen Evolution Reaction. *Adv. Funct. Mater.* **2017**, *27*, 1701825. [[CrossRef](#)]
19. Lu, X.; Lin, Y.; Dong, H.; Dai, W.; Chen, X.; Qu, X.; Zhang, X. One-Step Hydrothermal Fabrication of Three-dimensional MoS₂ Nanoflower using Polypyrrole as Template for Efficient Hydrogen Evolution Reaction. *Sci. Rep.* **2017**, *7*, 42309. [[CrossRef](#)]
20. Wang, H.; Lu, Z.; Kong, D.; Sun, J.; Hymel, T.M.; Cui, Y. Electrochemical Tuning of MoS₂ Nanoparticles on Three-Dimensional Substrate for Efficient Hydrogen Evolution. *ACS Nano* **2014**, *8*, 4940–4947. [[CrossRef](#)]
21. Najmaei, S.; Yuan, J.; Zhang, J.; Ajayan, P.; Lou, J. Synthesis and Defect Investigation of Two-Dimensional Molybdenum Disulfide Atomic Layers. *Acc. Chem. Res.* **2014**, *48*, 31–40. [[CrossRef](#)] [[PubMed](#)]
22. Lu, H.; Chen, X.; Dai, W.; Zhang, K.; Liu, C.; Dong, H. Prickly Pear-Like Three-Dimensional Porous MoS₂: Synthesis, Characterization and Advanced Hydrogen Evolution Reaction. *Catalysts* **2018**, *8*, 235. [[CrossRef](#)]
23. Gao, M.-R.; Chan, M.K.Y.; Sun, Y. Edge-terminated molybdenum disulfide with a 9.4-Å interlayer spacing for electrochemical hydrogen production. *Nat. Commun.* **2015**, *6*, 7493. [[CrossRef](#)] [[PubMed](#)]
24. Li, X.; Guo, S.; Li, W.; Ren, X.; Su, J.; Song, Q.; Sobrido, A.J.; Wei, B. Edge-rich MoS₂ grown on edge-oriented three-dimensional graphene glass for high-performance hydrogen evolution. *Nano Energy* **2019**, *57*, 388–397. [[CrossRef](#)]
25. Liu, J.; Yu, L.; Wu, C.; Wen, Y.; Yin, K.; Chiang, F.-K.; Hu, R.; Liu, J.; Sun, L.; Gu, L.; et al. New Nanoconfined Galvanic Replacement Synthesis of Hollow Sb@C Yolk-Shell Spheres Constituting a Stable Anode for High-Rate Li/Na-Ion Batteries. *Nano Lett.* **2017**, *17*, 2034–2042. [[CrossRef](#)]
26. Wang, Y.; Kang, W.; Cao, D.; Fan, X.; Yang, H.; Yang, Z.; Sun, D. Yolk-shell ZnS@NC@MoS₂ nanoboxes with enhanced sodium storage capability. *Appl. Surf. Sci.* **2022**, *574*, 151715. [[CrossRef](#)]
27. Stöber, W.; Fink, A.; Bohn, E. Controlled Growth of Monodisperse Silica Spheres in the Micron Size Range. *J. Colloid Interface Sci.* **1968**, *26*, 62–69. [[CrossRef](#)]
28. Li, X.-H.; Zhang, Y.-X.; Liu, Z.-L.; Liu, Q.-Z.; Li, B.; Zhu, G.-P.; Dai, K. A facile and novel approach for preparing monodispersed hollow aluminosilica microspheres with thin shell structures. *RSC Adv.* **2014**, *4*, 62209–62214. [[CrossRef](#)]
29. Yang, L.-Z.; Zhu, Y.-J.; Tong, H.; Liang, Z.H.; Wang, W.-W. Hierarchical β-Ni(OH)₂ and NiO Carnations Assembled from Nanosheet Building Blocks. *Cryst. Growth Des.* **2007**, *7*, 2716–2719. [[CrossRef](#)]
30. Yang, L.; Cui, X.; Zhang, J.; Wang, K.; Shen, M.; Zeng, S.; Dayeh, S.A.; Feng, L.; Xiang, B. Lattice strain effects on the optical properties of MoS₂ nanosheets. *Sci. Rep.* **2014**, *4*, 5649. [[CrossRef](#)]
31. Wang, C.; Lin, H.; Liu, Z.; Wu, J.; Xu, Z.; Zhang, C. Controlled Formation of TiO₂/MoS₂ Core-Shell Heterostructures with Enhanced Visible-Light Photocatalytic Activities. *Part. Part. Syst. Charact.* **2016**, *33*, 221–227. [[CrossRef](#)]
32. De Chialvo, M.R.G.; Chialvo, A.C. Hydrogen evolution reaction: Analysis of the Volmer-Heyrovsky-Tafel mechanism with a generalized adsorption model. *J. Electroanal. Chem.* **1994**, *372*, 209–223. [[CrossRef](#)]
33. Hu, J.; Huang, B.; Zhang, C.; Wang, Z.; An, Y.; Zhou, D.; Lin, H.; Leung, M.K.H.; Yang, S. Engineering stepped edge surface structures of MoS₂ sheet stacks to accelerate the hydrogen evolution reaction. *Energy Environ. Sci.* **2017**, *10*, 593–603. [[CrossRef](#)]
34. Luo, Z.; Ge, J.; Liu, C.; Xing, W. Engineering the HER catalytic behavior of heteroatom-doped molybdenum disulfide via versatile partial cation exchange. *J. Energy Chem.* **2020**, *41*, 15–19. [[CrossRef](#)]
35. Diao, L.; Zhang, B.; Sun, Q.; Wang, N.; Zhao, N.; Shi, C.; Liu, E.; He, C. An in-plane Co₉S₈@MoS₂ heterostructure for the hydrogen evolution reaction in alkaline media. *Nanoscale* **2019**, *11*, 21479–21486. [[CrossRef](#)]
36. Zhou, Q.; Zhao, G.; Rui, K.; Chen, Y.; Xu, X.; Dou, S.X.; Sun, W. Engineering additional edge sites on molybdenum dichalcogenides toward accelerated alkaline hydrogen evolution kinetics. *Nanoscale* **2019**, *11*, 717–724. [[CrossRef](#)]
37. Meng, X.; Yu, L.; Ma, C.; Nan, B.; Si, R.; Tu, Y.; Deng, J.; Deng, D.; Bao, X. Three-dimensionally hierarchical MoS₂/graphene architecture for high-performance hydrogen evolution reaction. *Nano Energy* **2019**, *61*, 611–616. [[CrossRef](#)]
38. Chi, J.-Q.; Gao, W.-K.; Lin, J.-H.; Dong, B.; Yan, K.-L.; Qin, J.-F.; Liu, B.; Chai, Y.-M.; Liu, C.-G. N,P dual-doped hollow carbon spheres supported MoS₂ hybrid electrocatalyst for enhanced hydrogen evolution reaction. *Catal. Today* **2019**, *330*, 259–267. [[CrossRef](#)]
39. Zhang, J.; Wang, T.; Liu, P.; Liu, S.; Dong, R.; Zhuang, X.; Chen, M.; Feng, X. Engineering water dissociation sites in MoS₂ nanosheets for accelerated electrocatalytic hydrogen production. *Energy Environ. Sci.* **2016**, *9*, 2789–2793. [[CrossRef](#)]
40. Chen, P.; Zhou, T.; Wang, S.; Zhang, N.; Tong, Y.; Ju, H.; Chu, W.; Wu, C.; Xie, Y. Dynamic Migration of Surface Fluorine Anions on Cobalt-Based Materials to Achieve Enhanced Oxygen Evolution Catalysis. *Angew. Chem. Int. Ed.* **2018**, *57*, 15471–15475. [[CrossRef](#)]